# 60 nm Widely Tunable Three Section Slot Laser

Jack Mulcahy, John McCarthy, Frank H. Peters, *Member, IEEE*, and Xing Dai, *Member, IEEE*

***Abstract*— This paper presents a tunable single mode Dual-mirror Slotted Fabry Pérot (DSFP) laser with near 60 nm tuning of the wavelengths between 1530 nm to 1590 nm. The laser modes measured demonstrate high SMSR lasing exceeding 30 dB with SMSRs as high as 45 dB. The electrical tuning of the laser facilitates more than 20 nm of continuous 50 GHz channel spacing between 1545 nm and 1565 nm. Additional thermal tuning facilitates more than 40 nm of continuous 50 GHz channel spacing between 1540 nm and 1580 nm.**

***Index Terms*— Tunable laser, photonic integrated circuit (PIC), slots, slotted mirror, monolithic integration.**

## I. Introduction

SINGLE mode semiconductor lasers have a wide variety of uses in optical communications with distributed feedback lasers (DFBs) often being used to fulfil this need. However the fabrication of DFBs requires high resolution lithography and complex regrowth which makes their production expensive and time consuming. For this reason laterally coupled DFB lasers [1], [2] and distributed Bragg reflector lasers (DBRs) [3], which require only a single growth, remain of interest. These devices typically require higher precision than standard photolithography allows, often using electron-beam lithography for patterning, which is expensive. On the other hand, by etching 1 µm reflective defects in a standard Fabry-Pérot (FP) laser cavity, single-mode semiconductor lasers can be created using standard lithographic practices [4], [5], [6], [7], [8]. The reflective defects are called "slots", a schematic of which is seen in Fig. 1. These slots offer additional reflective feedback within the cavity which restricts the allowed lasing wavelengths, turning a multi-mode Fabry Pérot (FP) into a single mode Slotted Fabry Pérot (SFP) [9]. The lasing wavelengths of this SFP are determined through the width and spacing of the slots making it possible to accomplish lasing with a side-mode suppression ratio (SMSR) of more than 30 dB by carefully adjusting the slot placements and slot number.

Through the use of slots a widely-tunable laser can be fabricated using photolithographic techniques with resolution no lower than 1 µm. Widely-tunable are key components for future optical telecommunications, with a single monolithically integrated tunable laser providing improved efficiency and performance [10]. Unlike lasers with nanoscale DFB gratings, the laser presented here requires no regrowth steps and no high resolution lithography. This laser achieves a high SMSR ($\geq$30 dB) through the use of two slotted waveguides as wavelength-selective reflective mirror sections surrounding a non-slotted waveguide which acts to provide gain to the laser structure.

This paper analyses slotted Fabry Pérot lasers consisting of a gain section and a slotted mirror section, and a gain section surrounded by two slotted mirror sections, which has been denoted as a Dual-mirror Slotted Fabry Pérot (DSFP). A comparison is made between the SFP and DSFP devices to highlight the benefit of the use of two asymmetric mirror sections. SFP lasers using two mirror sections [11] have previously been used to achieve a wide tuning range. In this paper we make use of the dual-mirror SFP design seen previously to create a laser which is capable of tuning across 60 nm from 1530 nm to 1590 nm by varying the bias of the three sections at 20 °C, in comparison to [11] which uses six electrically isolated sections. The design of this laser facilitates over 50 continuous channels with 50 GHz continuous spacing from 1545 nm to 1565 nm. By varying the temperature of the overall device from 20 °C to 30 °C over 100 continuous channels with 50 GHz continuous spacing from 1540 nm to 1580 nm can be obtained. We credit the enhanced tuning range and the accompanying continuity of the single mode output of the laser with the model we created to optimise the positioning of the slots in the two mirror sections. Through the modelling of the optimal mirror spacing pairs we were able to create a DSFP wherein the tuning of the emission mode can be broken down into a wider general tuning done by the left mirror section, and a finer tuning achieved via the right mirror section. This behaviour is explored and explained in Section III-B.

## II. Device Modelling

### A. Single Mirror Slotted Fabry Pérot Lasers

Slots operate by offering a minor reflective feedback as seen in Fig. 1. The light in the ridge waveguide is initially travelling in an effective refractive index $n_{WG}$. When light first encounters the slot, a small percentage of the light is reflected back due to a change in the effective index. The reflective slots in this device were etched down to just above the quantum wells and thus have a reflectivity of approximately 3% and a loss of 15% [12]. The light then enters a short 1 µm long waveguide, $L_S$, with effective refractive index $n_{slot}$. An isometric view comparison of a standard waveguide and a slotted waveguide is shown in Fig. 2.

Manuscript received 31 March 2023; revised 14 June 2023 and 9 August 2023; accepted 18 September 2023. Date of publication 25 September 2023; date of current version 6 November 2023. This work was supported by the Science Foundation Ireland under Grant 12/RC/2276 (IPIC). *(Corresponding author: Jack Mulcahy.)*

The authors are with the Tyndall National Institute, Cork, T12 R5CP Ireland, and also with the Physics Department, University College Cork, Cork, T12 CY82 Ireland (e-mail: jack.mulcahy@tyndall.ie).

Color versions of one or more figures in this article are available at https://doi.org/10.1109/JQE.2023.3318588.

Digital Object Identifier 10.1109/JQE.2023.3318588

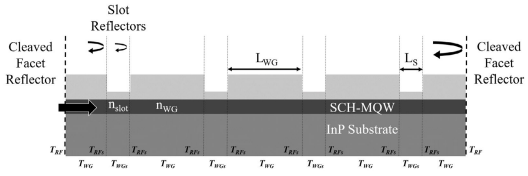


Fig. 1. A cross-sectional view of a slotted waveguide.

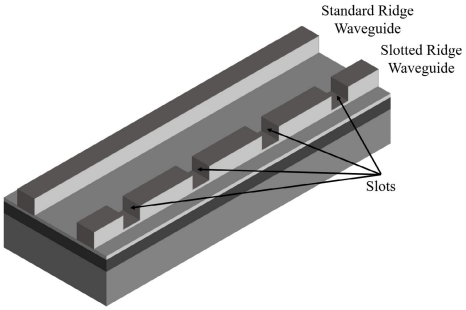


Fig. 2. A standard shallow-etched ridge waveguide versus a slotted waveguide.

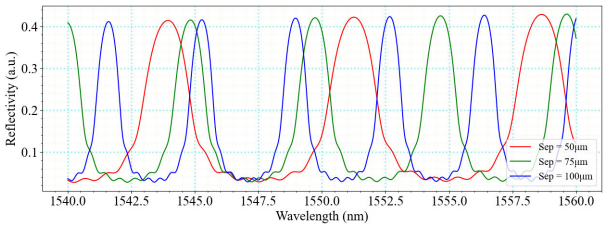


Fig. 3. The reflectivity versus wavelength for changing slot separations. The number of slots was fixed at 8 and the slot width was $0.88\mu m$.

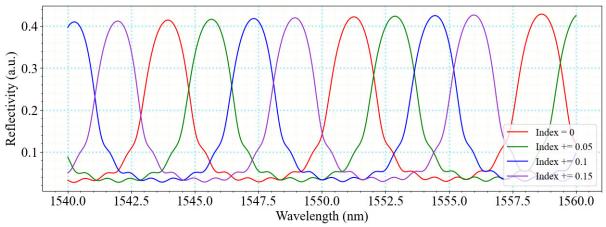


Fig. 4. A simulated view of a slotted mirror section with varying refractive indices. The slot separation was fixed at 50 μm.

The slot waveguide has a lower confinement factor than the ridge waveguide due to the reduced difference between the slot waveguide and the surrounding semiconductor. Thus the slot waveguide experiences more loss than the ridge waveguide. The light then encounters additional reflection when moving from the slot waveguide to the ridge waveguide, however this small reflected power experiences twice the loss of the slot waveguide. Thus the slots act to provide additional constraints on the lasing wavelength of a FP laser by dividing the total length of the etalon into a number of sections equal to one greater than the number of slots used. Fig. 2 shows 4 slots dividing a ridge into 5 sections.

A transfer matrix method can be used to determine the longitudinal-modal behaviour of a laser cavity [13]. A laser structure of length, $L$ and refractive index, $n_2$ surrounded by an index of $n_1$ can be represented as a series of reflectors ($RF$) and waveguides ($WG$). Thus a FP etalon, which consists of a waveguide cavity surrounded by two facets, can thereby be represented by multiplying the component matrices of the structure together;

$$\begin{aligned} T_{FP} &= T_{RF}\ T_{WG}\ T_{RF} \\ &= \frac{1}{t_{1,2}}\begin{pmatrix} 1 & r_{1,2} \\ r_{1,2} & r_{1,2}^2 + t_{1,2}^2 \end{pmatrix}\begin{pmatrix} e^{i\phi} & 0 \\ 0 & e^{-i\phi} \end{pmatrix} \cdot \\ &\quad \cdot \frac{1}{t_{2,1}}\begin{pmatrix} 1 & r_{2,1} \\ r_{2,1} & r_{2,1}^2 + t_{2,1}^2 \end{pmatrix} \end{aligned} \tag{1}$$

where $\phi = 2\pi nL/\lambda$ and the reflectivity and transmission of the second reflector has been altered to represent going from $n_2$ to $n_1$. Solving this equation results in a transfer matrix whose elements consist of the reflectivity, R, and transmission, T, of the etalon such that;

$$R = \left|\frac{T_{21}}{T_{11}}\right|^2 \quad T = \left|\frac{1}{T_{11}}\right|^2. \tag{2}$$

The reflectivity of a slotted laser can be calculated by considering the slot as a separate facet-waveguide-facet combination with 3% reflectivity, 15% loss and refractive index $n_{slot}$ that exists within the FP cavity as shown in Fig. 1. Using this technique, a slotted mirror (SM) section with one slot would have the transfer matrix form of

$$T_{S1} = T_{WG}\ T_{RF_S}\ T_{WG_S}\ T_{RF_S}\ T_{WG} \tag{3}$$

where the separation between slots is denoted with $WG$. This is noted in Fig. 1 as $L_{WG}$. The slot width is denoted with $WG_S$. This is noted in Fig. 1 as $L_S$. A SM section with N slots can therefore be written as

$$T_{SN} = T_{RF}\ T_{WG}\ \left(T_{RF_S}\ T_{WG_S}\ T_{RF_S}\ T_{WG}\right)^N\ T_{RF} \tag{4}$$

By numerically solving Eqn. 4 as a function of λ for $n = 3.217$ we can calculate the reflectivity $R(\lambda)$ for varying slot separations, $L_{WG}$. For the cleaved facet reflectors a lossless reflection of 33% was used. A slot width of 1 μm was used for $L_S$. We can see how the operating modes of the SM section depend heavily on the separation between each successive slot as shown in Fig. 3. Smaller separations lead to a wider wavelength spacing between resonant slotted-mirror modes as seen in red in Fig. 3 for a 50 μm separation. We refer to these slotted-mirror modes as "supermodes" to separate them from the longitudinal modes of a full etalon. Larger separations lead to narrower supermodes which are closer together as seen in blue in Fig. 3 for a 100 μm separation.

In addition, through the application of the electro-optic effect [5] or thermal effect [14], the refractive index of the SM section can also be controlled, the effect of which can be seen in Fig. 4. This effect changes the dominant lasing mode of the SFP [4]. In a DSFP both mirrors can be varied independently allowing the aligned mode to be controlled.

The introduction of slots into a regular FP cavity adds an additional constraint on the longitudinal modes which may resonate within the cavity to stimulate lasing. The transmission peaks of the original FP etalon which overlap the modal troughs of the slotted mirror's reflectivity become suppressed, which can prevent neighbouring modes from the wavelength of interest from lasing. Fig. 5 shows how the addition of three equally distributed slots along an FP etalon can alter

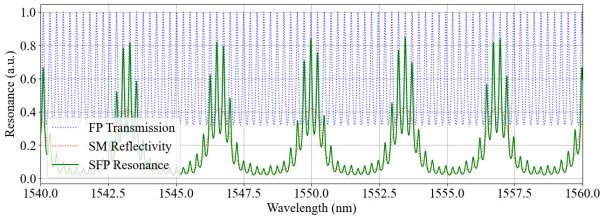


Fig. 5. Transmission of a 1500 µm cavity (blue), slots with a 108 µm separation (red), and the combined resonance (green).

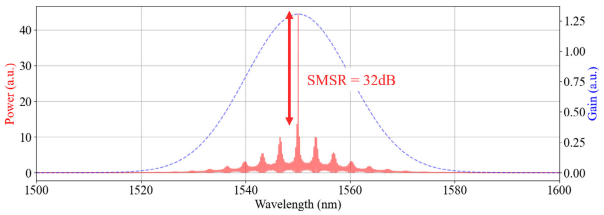


Fig. 6. The reflectivity of Fig. 5 with Gaussian gain as in Eqn. (5).

the laser transmission profile via the interaction between the cavity formed by the primary facets (blue) and the subcavities formed by the slots (red) to form an output (green) in which a majority of the FP modes are suppressed to facilitate single mode lasing. The cleaved facet reflectivity used is noted to affect the magnitude of this simulated output but not the peak wavelength positions.

Cassidy provides a relationship between the resonance of a cavity, $R_{SFP}(\lambda)$, and the resultant lasing power, $I_m^{\pm}(\lambda)$ [15]. Using this relationship we construct Eqn. (5), taking the total amount of spontaneous light which couples into the $m$ mode; $\delta_m = 1$, and using a Gaussian shape for the gain profile; $G(\lambda)$. We modulate the reflectivity of our SFP mirrors, $R_{SFP}(\lambda) = |r_{FP}r_{SN}|$ by the transmission of the total FP cavity formed by the device, $T_{FP}(\lambda)$. We transform the result into a an arbitrary decibel format to more closely resemble laser power measurements.

$$I_m^{\pm}(\lambda) = 10\log_{10}\left(\frac{<|\delta_m|^2>}{1 - R_{SFP}(\lambda)T_{FP}(\lambda)G(\lambda)}\right) \quad (5)$$

Now by transforming the reflective profile in Fig. 5 using Eqn. (5) we can see in Fig.6 how the immediate side-modes of what would be a FP cavity can be suppressed, producing a single mode laser with an SMSR of 32 dB.

### B. Dual-Mirror Slotted Fabry Pérot Lasers

When an FP etalon becomes an FP laser, each of these longitudinal modes has the same resonance which causes as many of them to lase simultaneously as the material gain of the laser allows. The supermodes present in the mirror section also have an equal resonance which means that when the SFP receives sufficient power multiple wavelengths will begin to lase simultaneously. This limits the single-mirror SFP to discontinuous tuning between the supermodes as tuning is achieved by changing the current across the gain section of the device. This effect can be overcome by using two SMs at either side of FP etalon to act as overlapping wavelength selective mirrors. By choosing SMs with different spacings, the modal selectivity of two SMs can be aligned to favour a

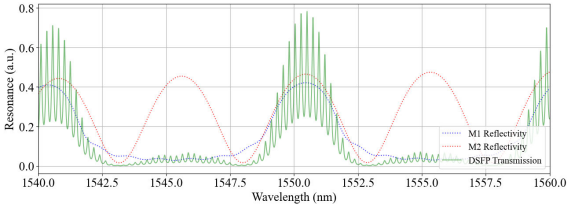


Fig. 7. A Dual-mirror slotted Fabry Pérot (DSFP) with total length 1600$\mu m$ (green). Mirror 1 has 36$\mu m$ slot separation (blue), Mirror 2 has 74$\mu m$ slot separation (red).

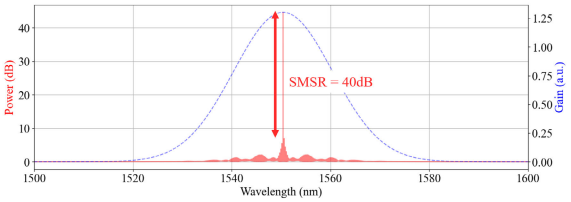


Fig. 8. Simulated available lasing modes of Fig. 7.


Fig. 9. A schematic view of the Single-mirror SFP device with slotted perturbations highlighted.

single one of the supermodes leading to the outer supermodes being suppressed. Fig. 7 shows an SFP with slot separation of 36 µm for the left mirror, $M_1$, with the addition of a secondary slotted mirror on the right, $M_2$, with a slot separation of 74 µm. It can be seen that now the supermodes generated by the slotted mirror are imbalanced with one wavelength, $\lambda = 1550.5$ nm, having the highest reflectivity.

Fig. 8 shows the resonance of Fig.7 converted into lasing modes using Eqn. 5. We can note that previous side-modes present in an SFP as shown in Fig. 6 are further suppressed by the usage of two slotted mirrors. This leads to a simulated 8 dB increase in the SMSR for our device when compared to Fig. 6 when using the same gain profile.

## III. Experimental Characterisation

### A. Single-Mirror Slotted Fabry Pérot Laser Testing

A single mirror SFP was fabricated by combining a slotted waveguide with an additional electrically isolated straight FP etalon as shown in Fig. 9. This laser consisted of a single cleaved facet on the right with reflectivity $\approx 33\%$ and a metal coated etched facet on the left with reflectivity $\approx 38\%$. The gain section had a length of 800 µm. The slotted mirror section acts as a wavelength selective mirror and is given enough power to be optically passive while the gain section is the main source of the laser's power output. The mirror section consisted of six slots spaced 108 µm apart. This device was measured by varying the current across these two sections with the device mounted on a temperature controlled chuck at 20 °C. A lensed optical fibre was used to couple light from the device into a into a Yokogawa optical spectrum analyser to measure the resultant spectra. This measurement was collected through a program written in LabVIEW which varied the current on each of the sections and collected a spectrum at each point of variance. The mirror section was

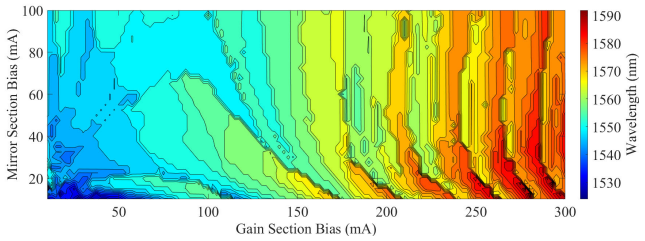


Fig. 10. An experimental measurement of a two section slotted device comparing section currents and the resultant wavelength.

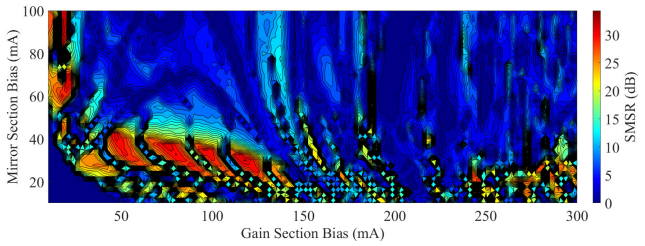


Fig. 11. An experimental measurement of a two section slotted device comparing section currents and the resultant SMSR.

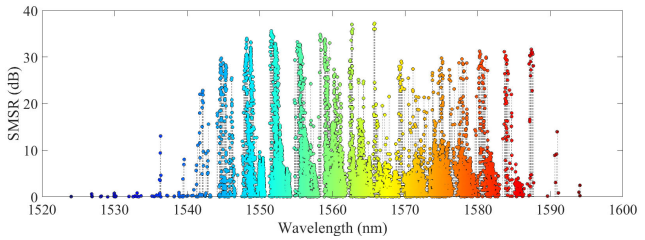


Fig. 12. Experimentally measured Wavelength vs SMSR for each collected spectrum of the SFP. Each point represents a collected spectrum for each bias point of the laser's two sections.

varied from 10 mA-100 mA with a step size of 5 mA. The gain section was varied from 20 mA-300 mA with a step size of 5 mA. 1008 spectra were collected of which 13.2% had an SMSR >30 dB.

Fig. 10 shows the resultant peak wavelengths obtained from experimental measurements of this SFP. Using a slotted mirror leads to an improvement in the SMSR compared to a regular FP laser and now allows us to tune between the supermodes present in the slotted mirror, similar to those shown in Fig. 5. Fig. 11 shows this single mode behaviour fails when the gain section or the mirror section receive higher currents. The peak wavelengths obtained from the device measurement compared to the resultant SMSR is shown in Fig. 12. In this graph each point represents a collected spectrum for each bias point of the laser's two sections. In this graph it can be seen how the laser's tuning is discontinuous across the supermodes. This limits both the continuity of the output laser spectrum and the widths of the lasers tunability across the spectrum.

### *B. Dual-Mirror Slotted Fabry Pérot Testing*

Using the device model presented in Section II-B a suitable combination of slot separations was designed to facilitate fabrication of a widely-tunable, high SMSR DSFP, whose design is shown in Fig. 13. This device is a 3 section laser with a central 800 µm waveguide section, referred to as the gain section, and two surrounding waveguide sections,

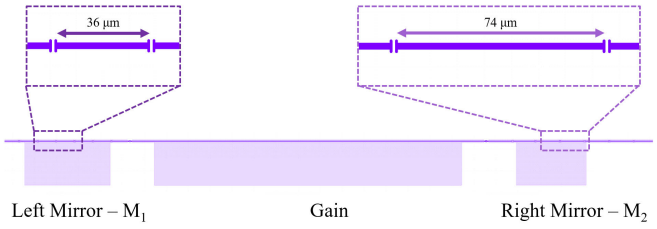


Fig. 13. A schematic view of the Dual-mirror Slotted Fabry Pérot (DSFP) device with slotted perturbations highlighted. A SEM image of a slot is included with slot separation of 1 µm.

each containing 6 slots, which will be referred to as mirror sections. The left mirror section, $M_1$, had a slot separation of 36 µm. The right mirror section, $M_2$, had a slot separation of 74 µm. Shorter spacings like 36 µm form supermodes that help to suppress active lasing modes further away from our wavelength of interest while larger separations like 74 µm form narrower supermodes which helps to suppress active modes closer to our wavelength of interest. Both effects are intended to act in tandem to help produce overall higher SMSR and more consistent single mode operation when compared to a single mirror slotted laser. These separations must also be chosen so that the supermodes created can align favourably over a single supermode when overlapped together as in Fig. 7. This laser consisted of a single cleaved facet on the right with reflectivity $\approx 33\%$ and a metal coated etched facet on the left with reflectivity $\approx 38\%$.

The device is based on a standard ridge waveguide semiconductor laser, separated into three active sections using slots etched into the ridge waveguide for electrical isolation between sections. The slots are formed in the same etch step as the ridge waveguide and while they do not penetrate the active region, their depth is sufficient to perturb the mode and cause a reflection. The reflections from each of the slot sections act as wavelength selective mirrors. The lasing wavelength is set by the overall resonance conditions which can be adjusted by varying the current injected into each section (and hence either the local refractive index or gain.) The longitudinal mode spacing of the device is set by the overall length of the device (1600 µm) with varying modes being preferentially selected due to the sectioning of the overall cavity.

The device was fabricated on commercially available lasing material consisting of 5 compressively strained AlGaInAs quantum wells of width 6 nm, on an n-doped InP substrate. The upper p-doped cladding consists of a 0.2 µm InGaAs cap layer, followed by 0.05 µm of InGaAsP, lattice matched to InP with a thickness of 1.62 µm. Standard lithographic techniques were used to define the ridge, with a ridge width of 2.5 µm, and height of 1.7 µm. Electrical isolation between different sections was achieved via similar slots as the ones used for optical feedback. All slots had a width of 1 µm. Electrical isolation slots were not coated in metal. Slots used for optical feedback were coated in a layer of Ti:Au to form electrically connected mirror sections. The shallow ridge etch ends above the quantum wells.

The DC characteristics of the device were first examined. The device was mounted on a temperature controlled chuck at 20 °C, and a lensed optical fibre was used to couple light

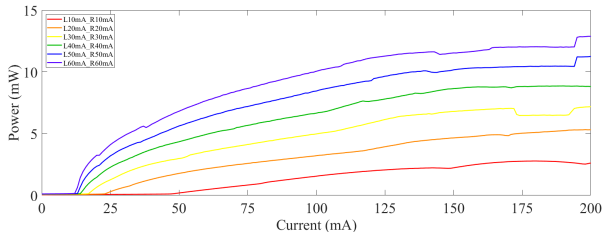


Fig. 14. An experimentally measured LI of the dual slot Fabry Pérot Laser with varying left (L) and right (R) mirror currents. LI measurements were taken with both mirror sections set at varying currents from 10 mA (red) to 60 mA (dark blue).

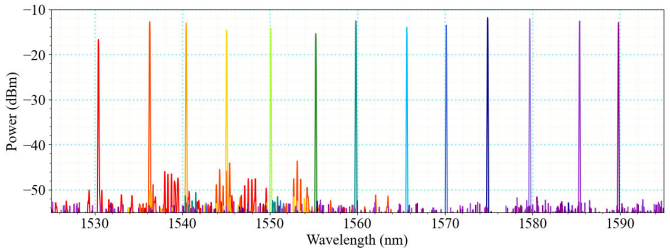


Fig. 15. A selection of experimentally measured spectra with ≈5 nm gaps showcasing some of the available lasing wavelengths. Each separate spectrum is denoted with a different colour.

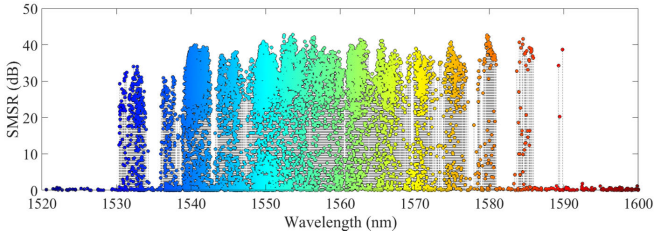


Fig. 16. Experimentally measured Wavelength vs SMSR for each collected spectrum of the DSFP. Each point represents a collected spectrum for each bias point of the laser's three sections.

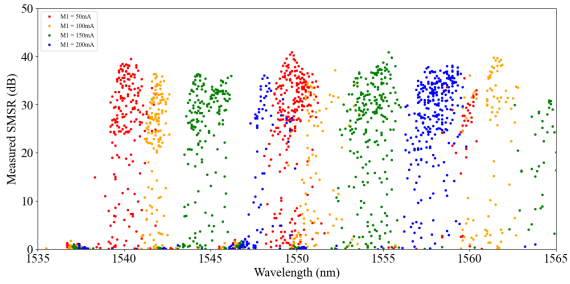


Fig. 17. Peak Wavelength vs SMSR measured from fixing the current in $M_1$ and varying the current in $M_2$ and the gain. Each $M_1$ current is represented by a different colour.

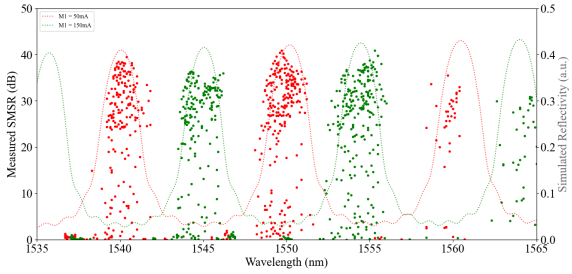


Fig. 18. A comparison of SMSR measured with simulated reflectivities for a 36 µm separation at $n = 3.217$ (red) and $n = 3.227$ (green).

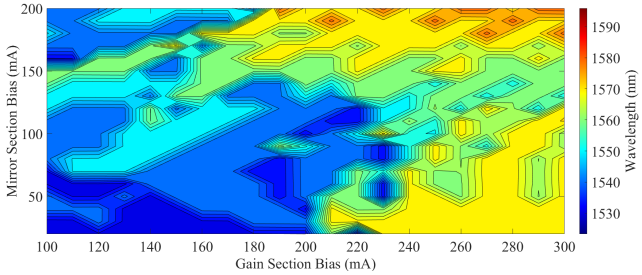


Fig. 19. Wavelength versus the current supplied to the gain section and $M_2$ when $M_1$ is fixed at 150 mA.

from the device. To test the LI output of the laser, the current through the gain section was swept while both surrounding mirror sections (mirror section I&II) were maintained at a set current. The current sweep on the gain section was repeated for varying mirror section currents. The results are shown in Fig. 14. The threshold of the laser can be seen to vary, depending on the current across the three sections with the smallest noted threshold being ≈ 12 mA.

The tuning of the DSFP involved varying the current across three different sections; the gain, the left mirror, and the right mirror. The light was then coupled into a lensed fiber and then into a Yokogawa optical spectrum analyser to measure the resultant spectra. This measurement was collected through a program written in LabVIEW which varied the current on each of these three sections and collected a spectrum at each point of variance. The mirror sections were each independently varied from 20 mA-200 mA with a step size of 10 mA. The gain section was varied from 20 mA-300 mA with a step size of 10 mA.

The total number of spectra obtained was 10469 of which 40.6% had an SMSR >30 dB, 30.1% had an SMSR between 30 dB and 20 dB, and 7.3% had an SMSR between 20 dB and 10 dB. An example of the spectra taken at 5 nm intervals is shown in Fig. 15, in which each spectrum is represented by a different colour. The full list of wavelengths obtained v.s the corresponding SMSR is shown in Fig. 16.

The selection of the wavelengths is determined by the current of mirror section; $M_1$. By setting the supermodes using the first mirror we generate a series of possible supermodes within which our main mode is capable of occurring. This behaviour is shown experimentally in Fig. 17 where we can see that when the spectra are divided by the current supplied to $M_1$, distinct grouping patterns become apparent. Using our previous simulation techniques we can see how these groupings correspond to the supermodes generated by $M_1$ as in Fig. 18. There exists a good agreement between the measured values and the reflectivity envelope generated by a slot spacing of 36 µm with $n = 3.217$ for a $M_1$ current of 50 mA and $n = 3.227$ for a $M_1$ current of 150 mA as shown. Similarly it can be shown that an $M_1$ current of 100 mA and 200 mA can be obtained using $n = 3.22$ and $n = 3.234$ respectively.

Tuning between these supermodes can be seen in Fig. 19. Increasing current in either section causes a minor change in wavelength until the next supermode becomes available. Fig. 20 shows that during the transition between these modes the SMSR of the device is reduced. This is similar to the two section SFP, however the key difference being that due to

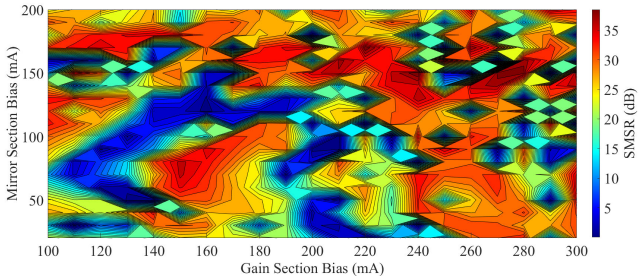


Fig. 20. SMSR versus the current supplied to the gain section and $M_2$ when $M_1$ is fixed at 150 mA.

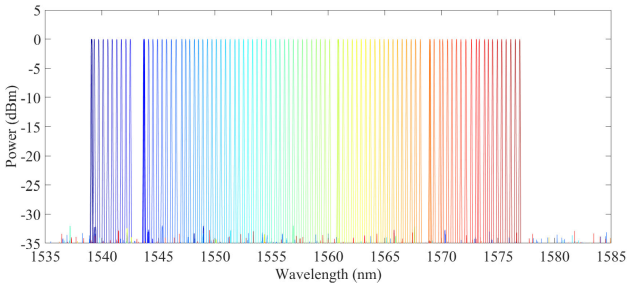


Fig. 21. Wavelength spread of the device with 50 GHz spacing. Spectra are normalised to 0 dB to accommodate for variations on power due to optical fibre drift during automated measurements.

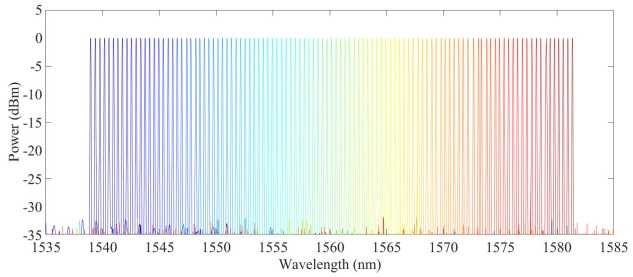


Fig. 22. Wavelength spread of the device with 50 GHz spacing with additional spectra taken from thermal tuning of the device. Spectra are normalised to 0 dB to accommodate for variations on power due to optical fibre drift during automated measurements.

the additional mirror, both the gain section and the secondary mirror section, $M_2$, can pumped to higher currents while still maintaining areas of high SMSR.

The ability to vary both sections while maintaining a high SMSR allows the DSFP to lase at a wide variety of wavelengths. Smaller variations in wavelength can be obtained by fixing both mirror sections and varying the current across the gain and larger changes in wavelength can be obtained by keeping $M_1$ fixed and varying the current across both the gain and $M_2$. This method of control on its own allows a full wavelength spread of nearly 60 nm and $>$ 20 nm of continuous 50 GHz channel spacings to be obtained within this tuning range as shown in Fig. 21. Spectra in this figure are normalised to compensate for a noted fibre drift which led to a decrease in fibre coupling over the course of the spectra collection. By introducing thermal variance into the system using the temperature controlled chuck at 25 °C and 30 °C the gaps present in this spread can be filled to create $>$ 40 nm of continuous 50 GHz channel spacing as seen in Fig.22.

## IV. Conclusion

A regrowth-free tunable single mode Dual-mirror Slotted Fabry Pérot (DSFP) laser based on asymmetric slotted mirrors is presented. The laser achieves a full tuning range of near 60 nm of the wavelengths between 1530 nm to 1590 nm. The laser produced high SMSR lasing $\geq$30 dB with SMSRs as high as 45 dB. The tuning of the laser facilitated $>$ 20 nm of continuous 50 GHz spacing with additional thermal tuning facilitating $>$ 40 nm of continuous 50 GHz spacing. A model used to design this laser is presented and is seen to align to the experimental behaviour of the laser. The accuracy of this model provides a template for lasers with single mode emission across the c-band, and by adjusting the placements of the slots in the mirror sections, laser designs for the o-band operation can also be produced using the same method. The methods used to design this laser offer a low-cost, low lithographic resolution ($\geq$1 µm) technique of single mode laser design.

## References

[1] L. M. Miller et al., "A distributed feedback ridge waveguide quantum well heterostructure laser," *IEEE Photon. Technol. Lett.*, vol. 3, no. 1, pp. 6–8, Jan. 1991.

[2] R. D. Martin et al., "CW performance of an InGaAs-GaAs-AlGaAs laterally-coupled distributed feedback (LC-DFB) ridge laser diode," *IEEE Photon. Technol. Lett.*, vol. 7, no. 3, pp. 244–246, Mar. 1995.

[3] R. M. Lammert, J. S. Hughes, S. D. Roh, M. L. Osowski, A. M. Jones, and J. J. Coleman, "Low-threshold narrow-linewidth InGaAs-GaAs ridge-waveguide DBR lasers with first-order surface gratings," *IEEE Photon. Technol. Lett.*, vol. 9, no. 2, pp. 149–151, Feb. 1997.

[4] B. Corbett and D. McDonald, "Single longitudinal mode ridge waveguide 1.3$\mu$m Fabry–Pérot laser by modal perturbation," *Electron. Lett.*, vol. 31, no. 25, pp. 2181–2182, Dec. 1995.

[5] J. Patchell, D. Jones, B. Kelly, and J. O'Gorman, "Specifying the wavelength and temperature tuning range of a Fabry–Pérot laser containing refractive index perturbations," *Proc. SPIE*, vol. 5825, pp. 1–13, Jun. 2005.

[6] S. O'Brien and E. P. O'Reilly, "Theory of improved spectral purity in index patterned Fabry–Pérot lasers," *Appl. Phys. Lett.*, vol. 86, no. 20, May 2005, Art. no. 201101.

[7] B. Kelly et al., "Discrete mode laser diodes with very narrow linewidth emission," *Electron. Lett.*, vol. 43, no. 23, pp. 1282–1284, Nov. 2007.

[8] R. Phelan et al., "A novel two-section tunable discrete mode Fabry–Pérot laser exhibiting nanosecond wavelength switching," *IEEE J. Quantum Electron.*, vol. 44, no. 4, pp. 331–337, Apr. 2008.

[9] H. Yang et al., "Monolithic integration of single facet slotted laser, SOA, and MMI coupler," *IEEE Photon. Technol. Lett.*, vol. 25, no. 3, pp. 257–260, Feb. 2013, doi: 10.1109/LPT.2012.2233197.

[10] B. Broberg and S. Nilsson, "Widely tunable active Bragg reflector integrated lasers in InGaAsP-InP," *Appl. Phys. Lett.*, vol. 52, no. 16, pp. 1285–1287, Apr. 1988, doi: 10.1063/1.99140.

[11] M. Nawrocka, Q. Lu, W.-H. Guo, A. Abdullaev, F. Bello, J. O'Callaghan, T. Cathcart, and J. F. Donegan, "Widely tunable six-section semiconductor laser based on etched slots," *Opt. Exp.*, vol. 22, pp. 18949–18957, Aug. 2014.

[12] Q. Y. Lu et al., "Analysis of slot characteristics in slotted single-mode semiconductor lasers using the 2-D scattering matrix method," *IEEE Photon. Technol. Lett.*, vol. 18, no. 24, pp. 2605–2607, Dec. 2006.

[13] L. Coldren, S. Corzine, and M. Mashanovitch, *Diode lasers and Photonic Integrated Circuits*. Hoboken, NJ, USA: Wiley, 2012, Ch. 3.

[14] S. Sakano, T. Tsuchiya, M. Suzuki, S. Kitajima, and N. Chinone, "Tunable DFB laser with a striped thin-film heater," *IEEE Photon. Technol. Lett.*, vol. 4, no. 4, pp. 321–323, Apr. 1992, doi: 10.1109/68.127200.

[15] D. Cassidy, "Analytic description of a homogeneously broadened injection laser," *IEEE J. Quantum Electron.*, vol. QE-20, no. 8, pp. 913–918, Aug. 1984.

[16] Y. Ueda, T. Shindo, S. Kanazawa, N. Fujiwara, and M. Ishikawa, "Electro-optically tunable laser with ultra-low tuning power dissipation and nanosecond-order wavelength switching for coherent networks," *Optica*, vol. 7, no. 8, p. 1003, 2020, doi: 10.1364/optica.392820.